tions using a similar edge. However, in his experiments, the edge was formed by a 1:5 ellipse instead of the one-quarter circle employed in the present investigation. Concerning the case of a nose-shape impingement corner geometry, the preferred event corresponds to "complete escape" of the approaching shear-layer vortex, as shown in the sequence of Figs. 2g and 2h. Moreover, the roll-up of the shear-layer vortical structures is generally incipient, implying that the arising vortices rarely achieve the maturity evidenced by those observed for the remaining geometries, hence facilitating a "complete escape."

The profiles of Reynolds normal and shear stresses are presented in Fig. 3, at different longitudinal stations in the cavity region. The time-averaged fluctuating flow characteristics are a result of random and periodic contributions that have not been decomposed in the present work. The development of the normal and shear stresses reveals a qualitatively similar distribution in the separated shear-layer region over the cavities, due to similar velocity fields and, hence, rates of strain. The magnitude of normal stresses increases very rapidly in the first cavity half. However, the variance of vertical fluctuating velocities displays much smaller peak values for the nose-shape edge geometry than for the remaining geometries. The results evince that the nose-shape geometry yields an effective reduction of the vertical oscillations amplitude. Based on flow visualization and time-averaged velocity characteristics, one can associate the ocurrence of vortex escape to a decrease in the maximum values of fluctuating velocities, while both partial and complete clipping contribute to the reinforcement of the vertical velocity fluctuations. Large differences in the time-averaged fluctuating velocity characteristics were measured inside the cavity mainly as a result of the different time-averaged flow structure.

Conclusions

Flow visualization and laser Doppler measurements have provided detailed information about the effect of the impingement edge geometry on both instantaneous and time-averaged characteristics of a cavity flow displaying organized oscillations. The use of three different downstream cavity edge geometries (sharp, nose-shape, and round) did not alter the corresponding Strouhal number value, $S_t = 1.1$, despite the fact that the recirculating flowfield inside the cavity was markedly influenced by the downstream corner geometrical detail. Attenuation of the fluctuation peak magnitudes was presented for the nose-shape impingement edge. The flow visualization bears that this attenuation is a direct consequence of the most frequent escape of the separated shear-layer vortices approaching the impingement edge.

References

[1]Sarohia, V., "Experimental Investigation of Oscillations in Flows Over Shallow Cavities," *AIAA Journal*, Vol. 15, No. 7, 1977, pp. 984–991.

[2]Rockwell, D., and Knisely, C., "The Organized Nature of Flow Impingement Upon a Corner," *Journal of Fluid Mechanics*, Vol. 93, Pt. 3, 1979, pp. 413–432.

[3]Knisely, C., and Rockwell, D., "Self-Sustained Low-Frequency Components in an Impinging Shear Layer," *Journal of Fluid Mechanics*, Vol. 116, March 1982, pp. 157–186.

[4]Rockwell, D., "Oscillations of Impinging Shear Layers," *AIAA Journal*, Vol. 21, No. 5, 1983, pp. 645–664.

[5]Durão, D. F. G., Heitor, M. V., and Pereira, J. C. F., "A Laser Anemometry Study of Separated Flow Over a Model Three-dimensional Hill," *Applications of Laser Anemometry to Fluid Mechanics*, edited by R. J. Adrian, T. Asanuma, D. F. G. Durão, F. Durst, and J. H. Whitelaw, Springer-Verlag, Berlin, 1989, pp. 93–118.

[6]Durst, F., Melling, A., and Whitelaw, J. H., *Principles and Practice of Laser-Doppler Anemometry*, 2nd. ed., Academic Press, New York, 1981, Chap. 7.

[7]Yanta, W. J., and Smith, R. A., "Measurements of Turbulent-Transport Properties with a Laser-Doppler Velocimeter," AIAA Paper 73-169, 1978.

[8]Rockwell, D., "Prediction of Oscillation Frequencies for Unstable Flow Past Cavities," *ASME Journal of Fluids Engineering*, Vol. 99, No. 2, 1977, pp. 294–300.

[9]Rockwell, D., and Knisely, C., "Vortex-Edge Interaction: Mechanisms for Generating Low Frequency Components," *Physics of Fluids*, Vol. 23, No. 2, 1980, pp. 239, 240.

[10]Ethembabaoglu, S., "On the Fluctuating Flow Characteristics in the Vicinity of Gate Slots," Div. of Hydraulics Engineering, Univ. of Trondheim, Norwegian Inst. of Technology, Norway, June 1973.

Comparative Study of Higher Order Turbulence Models for Compressible Separated Flows

C. C. Chuang* and C. C. Chieng†
National Tsing Hua University,
Hsinchu, Taiwan 30043, Republic of China

I. Introduction

ALTHOUGH turbulent separated flow has been the subject of many studies in the past few years, little of the reported research addressed high speed, as it related to the processes of separation, shear layer development, reattachment, and interaction of shock wave/separation. Predicting compressible turbulent separation is challenging both numerically and physically because the application of higher order turbulent closures requires solving highly coupled and nonlinear transport equations. Most studies use the algebraic turbulence models to eliminate the complexity of numerical and physical modeling. Recently, several investigations have incorporated a k-ϵ two-equation turbulence model when solving for transonic flows over bumps,[1,2] where the results showed an underestimation of shock-wave/boundary-layer interaction and a mismatch in the measured and computed shock location. An algebraic stress model (ASM) has also been successfully implemented and improves the predictions for the same problems.[2] Extensive experience in the incompressible environment suggests that second moment closure turbulence models are necessary for a satisfactory prediction of recirculating, curved flows.[3] Use of the second moment closure model sharply increases the difficulty in numerical stability arising from the stiff problem near the wall. Therefore, the solution algorithm is important in achieving convergence with high accuracy.

The objective of the present study was to examine the performance of Chien's low Reynolds number k-ϵ turbulence model,[4] ASM/k-ϵ two-layer model,[2] and Shima's near-wall Reynolds stress model[5] for predicting the transonic shock-induced separated flowfields over bump. Chien's k-ϵ model was chosen because of its simplicity, easy implementation, and stability when applied to complex flows. The inclusion of the high anisotropic effect of the turbulent stresses in the immediate vicinity of wall and the easy assessment of the empirical constants for the pressure-strain term are the reasons for choosing Shima's Reynolds stress model for this study.

II. Physical and Mathematical Models

The governing equations used to describe the mean flow for this study are the time-dependent, mass-averaged, compressible Navier-Stokes equations. Depending on the two-equation k-ϵ model or Reynolds stress turbulence model used, the mean flow equations are augmented by additional transport equations of (k and ϵ) or ($\overline{u_i' u_j'}$ and ϵ) where k, ϵ and $\overline{u_i' u_j'}$ are the turbulent kinetic energy, dissipation rate, and Reynolds stress components. The governing equation written in vector form in the (ξ, η) coordinate system can be expressed as

$$\partial_t(\hat{Q}) + \partial_\xi(\hat{E} - \hat{E}_v) + \partial_\eta(\hat{F} - \hat{F}_v) + j(\hat{H} - \hat{H}_v) = \hat{W} \qquad (1)$$

Received Aug. 24, 1993; revision received March 11, 1994; accepted for publication March 14, 1994.

*Graduate Student, Department of Power Mechanical Engineering.
†Professor, Department of Nuclear Engineering. Member AIAA.

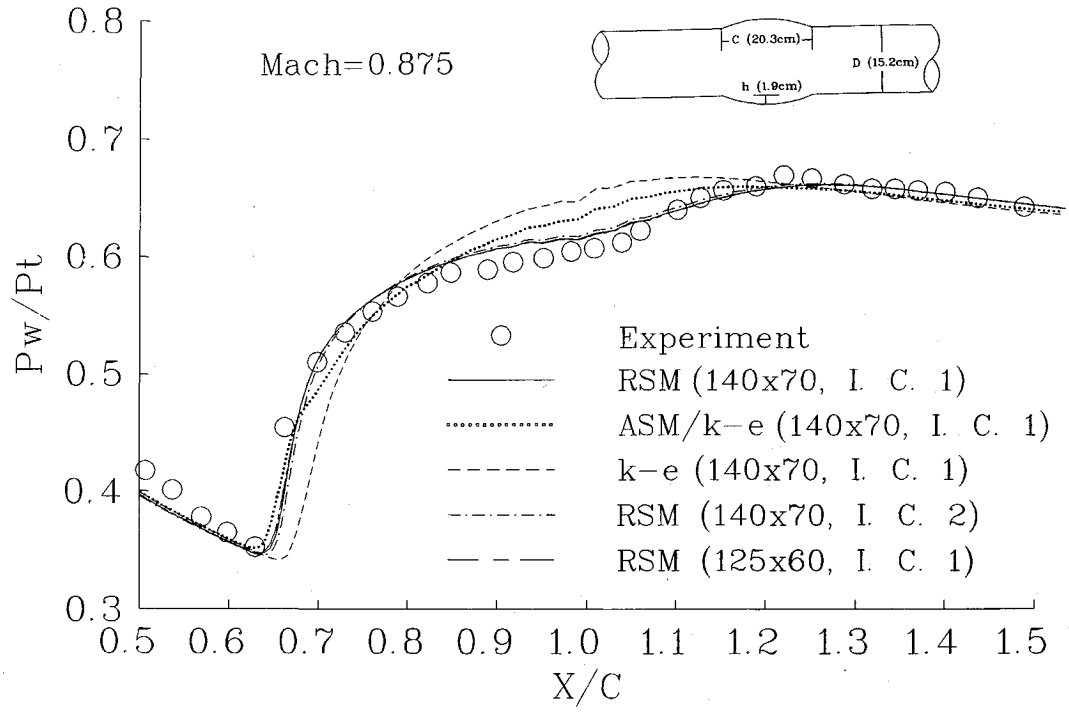

Fig. 1 Surface pressure distributions for different turbulent models and inflow conditions, $M_1 = 0.875$.

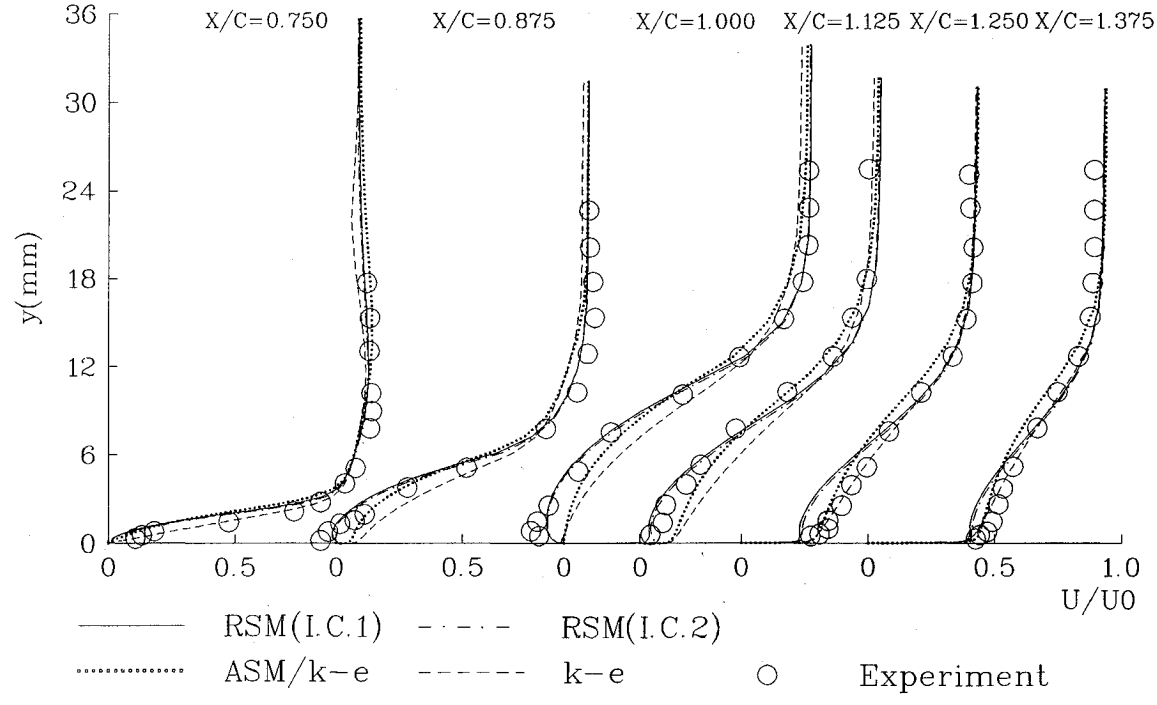

Fig. 2 Velocity profiles at various axial stations, $M_1 = 0.875$.

Equation (1) describes two-dimensional flow if $j=0$ and axisymmetric flow if $j=1$, where $\boldsymbol{Q}$ is the vector of dependent variables. $\hat{\boldsymbol{Q}} = \boldsymbol{Q}/J = J^{-1}\{\rho, \rho u, \rho v, e, \rho k, \rho\epsilon\}$ for both the k-ϵ turbulent model and the ASM/k-ϵ two-layer model. However, the vector expands to $\hat{\boldsymbol{Q}} = \boldsymbol{Q}/J = J^{-1}\{\rho, \rho u, \rho v, e, \rho\overline{u'v'}, \rho\overline{u'u'}, \rho\overline{v'v'}, \rho\overline{w'w'}, \rho\epsilon\}$ if Shima's Reynolds stress model is applied. The vectors of $\hat{\boldsymbol{E}}$ and $\hat{\boldsymbol{F}}$ represent corresponding convective fluxes and contain the convection and pressure terms, but the vectors of $\hat{\boldsymbol{E}}_v$ and $\hat{\boldsymbol{F}}_v$ describe diffusive fluxes. The vectors of $\hat{\boldsymbol{H}}$ and $\hat{\boldsymbol{H}}_v$ are the source terms of convection, diffusion, and turbulent energy associated with axisymmetric coordinates, whereas $\hat{\boldsymbol{W}}$ contains the source term for production, destruction, and redistribution of turbulent energy. J is the Jacobian, and the perfect gas equation of state is added to complete the system of equations.

III. Numerical Methods

Additional turbulent equations make the system of governing equations not only larger but also stiffer and is difficult to solve. For considerations of numerical accuracy and stability, Harten's second-order upwind TVD scheme[6] was employed to discretize the convection terms of the mean flow equations and turbulence

transport equations. Thus the governing equations yield a difference equation set of nonfactored form as follows:

$$\boldsymbol{A}_{i,j}(\Delta\boldsymbol{Q})_{i-1,j}+\boldsymbol{C}_{i,j}(\Delta\boldsymbol{Q})_{i+1,j}+\boldsymbol{E}_{i,j}(\Delta\boldsymbol{Q})_{i,j-1}$$
$$+\boldsymbol{F}_{i,j}(\Delta\boldsymbol{Q})_{i,j+1}+\boldsymbol{D}_{i,j}(\Delta\boldsymbol{Q})_{i,j}=\boldsymbol{B}_{i,j} \quad (2)$$

Equation (2) is a diagonal-dominated block pentadiagonal matrix system of equations. The unknowns $(\Delta\boldsymbol{Q})_{i,j}$ were conventionally evaluated by using the block Gauss-Seidel method with slow convergence. Several variants of biconjugate gradient algorithms with a preconditioner of incomplete lower/upper-factorization (ILU) have been tested with success when employed with the two-equation k-ϵ turbulence model.[8] The present study extends the same numerical method of Bi-CGSTAB[7] for both the application of the ASM/k-ϵ two-layer model and the Reynolds stress model with larger vectors of $\boldsymbol{B}$, $\Delta\boldsymbol{Q}$ (9×1) and matrices of $\boldsymbol{A}$, $\boldsymbol{C}$, $\boldsymbol{D}$, $\boldsymbol{E}$, and $\boldsymbol{F}$ (9×9).

IV. Results and Discussion

Numerical computations have been made for the case of transonic shock-induced separated flow over an axisymmetric bump, at a freestream Mach number of 0.875 and a unit Reynolds number of 13.6×10^6/m (Refs. 1 and 9). Two grid systems of 140×70 and 125×60, clustered near the shock location and the wall with a minimum y^+ of 0.5, are used to test the grid independence. If the ASM/k-ϵ two-layer model is used, 15 points are set in the inner layer corresponding to minimum turbulent Reynolds number ($P\sqrt{k}y/\nu$) of 200 to ensure enough resolution in the viscous sublayer. In the flow direction, the boundaries of the computational domain extend from -4C to 4C. Moreover, two inflow turbulent properties of $k_{0,1}=1.5(0.02V_\infty)^2$, $\epsilon_{0,1}=(k_{0,1})^{1.5}/0.01$, and $k_{0,2}=4(k_{0,1})$, $\epsilon_{0,2}=(k_{0,2})^{1.5}/0.01$ (denoted as I.C.1 and I.C.2 in the figures) are applied to test the influence of inlet conditions. The results show that only slight difference of mean and turbulent properties are present for these two inlet conditions and grid systems.

Figure 1 shows a schematic diagram of the bump and the comparison of surface pressure distributions. The wall pressure distribution near the shock location is reproduced with good accuracy by the Reynolds stress model and ASM/k-ϵ two-layer model. The two-equation k-ϵ model predicts the shock location somewhat downstream and underestimates the shock-induced interaction strength. As for the pressure prediction along the recirculating region downstream of the strong shock-wave/boundary-layer

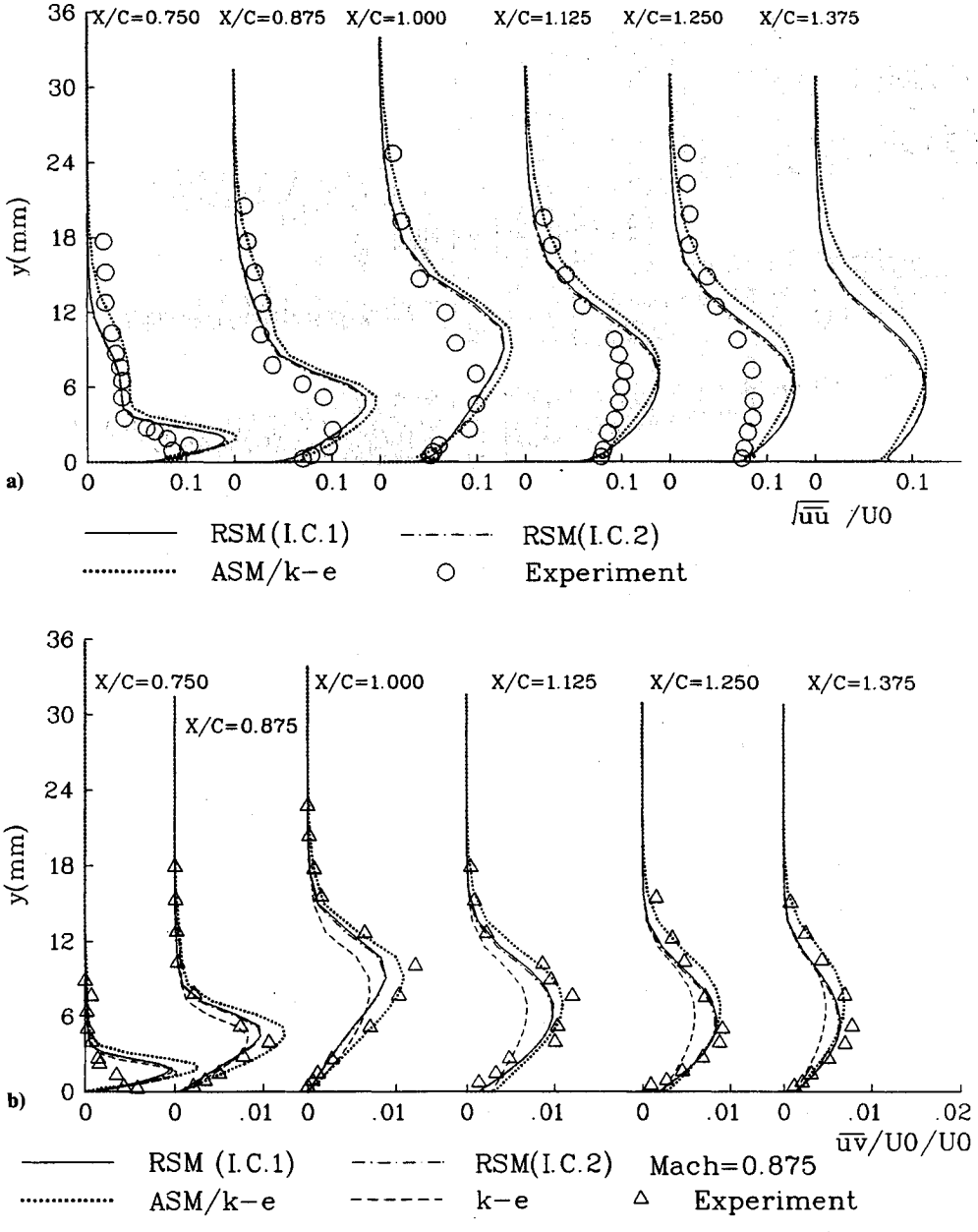

Fig. 3 Computed and measured profiles: a) Streamwise turbulent stress profiles and b) Reynolds shear stress profiles at various axial stations, $M_1=0.875$.

interaction, the Reynolds stress model that imposes both the convective and diffusive effects of Reynolds stresses does produce the best agreement with experimental data among these turbulence models, although both the Reynolds stress model and algebraic stress model give similar accuracy in predicting the shock location.

Figure 2 shows the comparisons of the velocity profiles in the postshock separated region and the recovering zone following reattachment by various turbulence models. The differences especially near the wall region show the ability of these models to capture the separation process. The Reynolds stress model predicts best the start of separation and the separation process, however, the broad recirculation bubble also implies the underestimation of the velocity during flow redevelopment and an insufficient rate of recovery. The k-ϵ two-equation model reveals an insufficient level of interaction and thus fails to capture the onset of separation and gives a smaller recirculation region, but the smaller recirculating zone gives the "appearing good" agreement of the velocity profiles with measurement in the redeveloping region. The ASM/k-ϵ model induces separation earlier than the eddy viscosity model but slightly later than the Reynolds stress model. Also, the Reynolds stress model has the greatest sensitivity to the shock, the ASM/k-ϵ two-layer model exhibits a little less sensitivity to the shock, and the k-ϵ two-equation model gives the least sensitivity of the boundary layer to the shock.

It is expected that the shock and the velocity gradients in the separated region can elevate the streamwise turbulent stress by the contribution of streamwise strain to turbulent production, but the contribution is somewhat overestimated by these turbulence models when the computed profiles are compared with measured profiles (Fig. 3a). However, the predicted turbulent shear stress distribution at selected streamwise stations agree with measurement in terms of magnitudes with a little mismatch of peak locations (Fig. 3b). It also shows that both the Reynolds stress model and the ASM/k-ϵ two-layer model, which include the anisotropic effects of turbulent properties, obtain better predictions of the Reynolds shear stress than the eddy-viscosity, two-equation k-ϵ turbulence model.

The convergence and stability of the computational method is another concern of the present study. When the computations were performed on the CONVEX 3460, the computational efficiencies for the Reynolds stress model, ASM/k-ϵ model, and k-ϵ model are 4.13×10^{-4}, 3.90×10^{-4}, and 3.67×10^{-4} CPU s/grid/iteration, respectively. The L_2 residuals can be reduced to 3×10^{-9} after about 4000 iteration time steps which correspond to a total CPU time of about 5–6 h. It is noted that the computation is started from the freestream initial conditions and no prerun or other special treatment is necessary for initial guess of flowfield. Also, the computations are performed with the higher order closure turbulence models from the first time step, which is different from other investigations. Other computations usually start with an algebraic turbulence model until a nearly converged solution is obtained, and then continue with the higher order closure turbulence model.

V. Conclusions

Conclusions regarding the present study can be made as follows:

1) The Reynolds stress model has the best performance in predicting the onset of the separation process, mean velocity profiles, and turbulent normal and shear stresses in the separated region for the test case. The Reynolds stress model does predict the mean flowfield very well but needs further improvement in predicting turbulent quantities in the regions near the shock or expansion wave. All three turbulence models underestimate the recovery rate of mean flowfields in the redeveloping region.

2) The numerical method can perform the computation for compressible, complex turbulent, separated flow with high accuracy and a fast convergence rate.

Acknowledgment

The authors want to thank the National Science Council of Republic of China for its support under Contract NSC-82-0413-E-007-109.

References

[1]Johnson, D. A., Horstman, C. C., and Bachalo, W. D., "Comparison Between Experiment and Prediction for a Transonic Turbulent Separated Flow," *AIAA Journal*, Vol. 20, No. 6, 1982, pp. 737–744.

[2]Chuang, C. C., and Chieng, C. C., "Transonic Turbulent Separated Flow Predictions Using a Two-Layer Turbulent Model," *AIAA Journal*, Vol. 31, No. 5, 1993, pp. 816, 817; also AIAA Paper 92-0518, Jan. 1992.

[3]Launder, B. E., "Second-Moment Closure: Present and Future?" *International Journal of Heat and Fluid Flow*, Vol. 10, No. 4, 1989, pp. 282–299.

[4]Chien, K. Y., "Prediction of Channel and Boundary-Layer Flows with a Low-Reynolds-Number Turbulence Model," *AIAA Journal*, Vol. 20, No. 1, 1982, pp. 33–38.

[5]Shima, N., "A Reynolds-Stress Model for Near-Wall and Low-Reynolds-Number Regions," *Journal of Fluids Engineering*, Vol. 110, March 1988, pp. 38–44.

[6]Yee, H. C., and Harten, A., "Implicit TVD Scheme for Hyperbolic Conservation Laws in Curvilinear Coordinates," AIAA Paper 85-1513, July 1985.

[7]Van Der Vorst, H. A., "Bi-CGSTAB: A Fast and Smoothly Converging Variant of Bi-CG for the Solution of Nonsymmetric Linear Systems," *SIAM Journal of Scientific and Statistical Computing*, Vol. 13, No. 2, 1992, pp. 631–644.

[8]Lin, H., Yang, D. Y., and Chieng, C. C., "Variant Bi-Conjugate Gradient Methods for Compressible Navier-Stokes Solver with a Two-Equation Model of Turbulence," AIAA Paper 93-3316, July 1993.

[9]Bachalo, W. D., and Johnson, D. A., "Transonic, Turbulent Boundary-Layer Separation Generated on an Axisymmetric Flow Model," *AIAA Journal*, Vol. 24, No. 3, 1986, pp. 437–443.

Effect of Isotropy of Actuation Strains for a Plate with a Hole

Mohammed H. Kadivar,* K. Pradeep Sensharma,† and Raphael T. Haftka‡
Virginia Polytechnic Institute and State University, Blacksburg, Virginia 24061

Introduction

FOR a plate with a hole subject to uniform tension at its ends, there will be stress concentration around the hole. Shape memory alloys and piezoelectric materials can be used as induced strain elements to reduce stresses in the regions of stress concentration by applying energy, usually electric current. Sensharma et al.[1] showed that when isotropic actuation strains are applied in a ring centered at the hole, the stresses will not change in the interior of the ring. They also found numerically that when the actuation strains are anisotropic, the stresses in the interior of the ring will change. The objective of this work is to confirm analytically these results.

General Equations

For an isotropic plate subjected to actuation strains in the radial ε_{ir} and tangential $\varepsilon_{i\theta}$ directions, Hooke's law may be written as

$$\varepsilon_r = \frac{1}{E}(\sigma_r - \nu\sigma_\theta) + \varepsilon_{ir}$$
$$\varepsilon_\theta = \frac{1}{E}(\sigma_\theta - \nu\sigma_r) + \varepsilon_{i\theta} \quad (1)$$

Received March 18, 1993; revision received Feb. 10, 1994; accepted for publication Feb. 21, 1994.

*Visiting Professor, Mechanical Engineering Department; currently Associate Professor, Engineering School, Shiraz University, Shiraz, Iran.

†Graduate Research Assistant, Department of Aerospace and Ocean Engineering.

‡Christopher C. Kraft Professor, Department of Aerospace and Ocean Engineering. Associate Fellow AIAA.